Oscillations of Drops with Mobile Contact Lines on the International Space Station: Elucidation of Terrestrial Inertial Droplet Spreading

J. McCraney, V. Kern, J. B. Bostwick, S. Daniel, and P. H. Steen

Phys. Rev. Lett. **129**, 084501 — Published 16 August 2022

DOI: 10.1103/PhysRevLett.129.084501

Oscillations of drops with mobile contact-lines on the International Space Station inform inertial wetting

J. McCraney,[1] V. Kern,[1] J.B. Bostwick,[2] S. Daniel,[1] and P.H. Steen[1]

[1]*Robert Frederick Smith School of Chemical and Biomolecular Engineering, Cornell University, Ithaca, NY, 14853, USA*
[2]*Department of Mechanical Engineering, Clemson University, Clemson, SC, USA*

(Dated: June 9, 2022)

We analyze shape oscillations of sessile water drops with fully mobile contact-lines (CL) aboard the International Space Station (ISS). The unique microgravity environment enables the study of centimeter-sized droplets with associated inertial-capillary motions. Plane-normal substrate vibrations induce resonance behaviors quantified by frequency scans from which the natural frequencies and mode shapes are identified for nine different hydrophobic surfaces. Experimental observations agree well with, and validate, a recent spectral prediction of mobile CL sessile drop oscillations. The experimental findings help elucidate terrestrial droplet inertial spreading, a poorly understood phenomenon pervasive in many processes.

Droplet motions on substrates are intrinsic to numerous industrial processes and technologies, such as step and imprint lithography in semiconductor manufacturing [1], additive manufacturing [2], spray cooling [3], drop impacts [4–6], and the assembly of autonomous fluidic machines [7]. The sessile drop is the canonical problem upon which the aforementioned applications are based and highlights the inherent multiphysics in inertial wetting phenomena. In classifying the dynamics, drops can move on a contacting surface with relative ease (free drops), others resist surface movement and spread/recede slowly (partially-free drops), while others do not move on the surface (pinned drops). This range of behaviors can be quantified by the mobility Λ of the three-phase CL which is unique to the particular liquid-solid-gas system and flow conditions. On Earth, drop CL displacements are on the order of 50 μm and of similar scale to the surface roughness, making experimental realization of fully-mobile CLs nearly impossible, with the closest exception being slippery liquid-infused porous surfaces (SLIPS) [8–10]. However, in microgravity it is possible to overcome such defects to generate fully mobile CL conditions $\Lambda = 0$. In this Letter, we report an experimental study from the ISS of sessile drop oscillations with fully-mobile CLs, enabled by flow conditions realized in microgravity. This critical insight enables precise predictions of CL spreading, pervasive throughout terrestrial processes, but which has largely eluded experimental analysis.

A sessile drop in equilibrium is defined by the base radius a and static contact-angle (CA) α, as shown in Figure 1**a**. Shape oscillations can be excited by plane-normal vibrations of the substrate, which induce contact-line (CL) motions with physics governed by a constitutive relationship relating CA deviations $\Delta\alpha$ to the contact-line speed u_{CL} (cf. Figure 1**b**), which upon linearization about $u_{CL} = 0$ yields the Davis-Hocking [11, 12] dynamic contact-line law

$$\Delta\alpha = \Lambda u_{CL}. \tag{1}$$

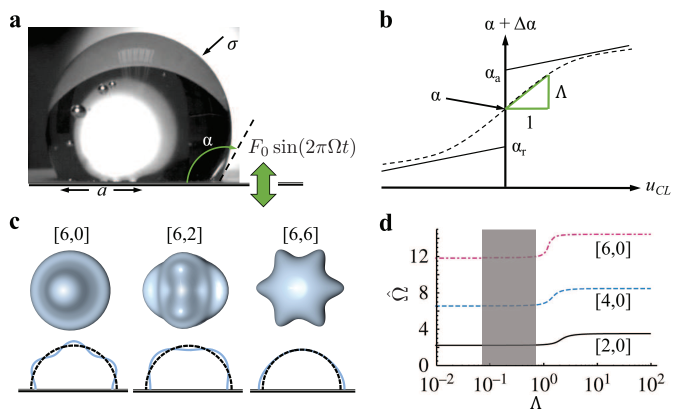

FIG. 1: **a** Definition sketch of driven sessile drop with base radius a and contact-angle α whose contact-line obeys **b** a dynamic contact-line law which relates α to the contact-line speed u_{CL} through the contact-line mobility parameter Λ and advancing α_a and receding α_r contact angles. **c** Under resonant conditions, the drop will oscillate with characteristic frequency Ω and shape defined by the mode number pair $[k, l]$ classified using spherical harmonic terminology into zonal $[6, 0]$, tesseral $[6, 2]$, and sectoral $[6, 6]$ shapes. **d** Theoretical prediction of the scaled oscillation frequency $\hat{\Omega}$ for the first three axisymmetric modes against mobility Λ for $\alpha = 105°$ illustrates the limiting cases of the fully mobile $\Lambda = 0$ and pinned $\Lambda = \infty$ contact-line, with the shadowed region denoting the experimental parameter range.

Here Λ is the contact-line mobility, sometimes referred to as a homotopy parameter such that $\Lambda \in [0, \infty]$ with limiting cases of i) $\Lambda = 0$ a fully mobile CL (fixed CA) and ii) $\Lambda = \infty$ pinned CL. Intermediate cases $\Lambda \neq 0, \infty$ exhibit finite CL mobility and can induce dissipation, even in inviscid fluids. Bostwick and Steen [13] computed the frequency spectrum from an operator equation,

$$\hat{\Omega}^2 M[y] = K[y], \tag{2}$$

showing how the scaled drop frequency $\hat{\Omega} \equiv 2\pi\Omega\sqrt{\sigma/\rho a^3}$ depends upon the wetting parameters $\hat{\Omega}_{[k,l]}(\alpha, \Lambda)$ where

ρ and σ are density and surface tension. The corresponding mode shapes $y_{[k,l]}$ are defined by the mode number pair $[k, l]$ inherited from the spherical harmonics [14], as shown in Figure 1**c**. Steen et al. [15] have recast the problem using a symmetry-breaking perspective and showed how the sessile drop spectrum can be organized into a ‘periodic table of droplet motions’, making an analogy with the periodic table of chemical elements. Theoretical predictions include splitting of the Rayleigh drop degeneracy [16], spectral reordering, and mode mixing, all of which have been experimentally verified by Chang et al. [17, 18], who have observed the first 37 resonance modes for pinned CL conditions $\Lambda = \infty$. Enforcing pinned CL conditions experimentally can be achieved either through i) mechanical pinning of the CL by a finite-sized surface defect or ii) using high CA hysteresis surfaces, which effectively immobilizes the CL for small interface disturbances [19, 20]. Pinned CLs are common in drop oscillation experiments [21–23]. In contrast, the observation of fully mobile contact-line motions $\Lambda = 0$ has been elusive, with the notable exception of the recent study by Xia and Steen [24] that was focused on CL motions with finite mobility $\Lambda \neq 0, \infty$.

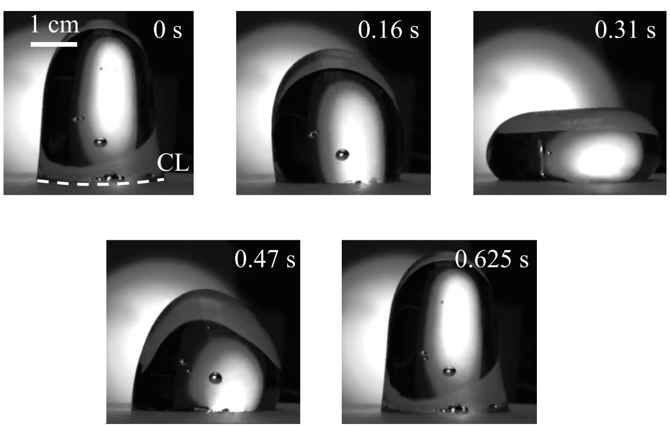

FIG. 2: Droplet driven at 1.6 Hz oscillating in the [2,0] mode on Substrate F_3 exhibits a freely moving contact-line.

Our experimental study fills this gap by leveraging the unique microgravity environment aboard the ISS. The advantage of microgravity is the magnification of the capillary length $\ell = \sqrt{\sigma/\rho g}$ and time $t_c = \sqrt{\rho a^3/\sigma}$ scales. On Earth $\ell = 3$ mm, but since $\ell \sim 1/\sqrt{g}$, the microgravity acceleration $g \sim 10^{-6}$ m/s^2 implies $\ell \sim 1$ m, allowing for experimentation with centimeter-sized drops, 10 times larger than those typically used in terrestrial conditions, with corresponding 30 fold amplification in time scale. The ISS is enabling, allowing for accurate spatial and temporal resolution of the CL dynamics, particularly for hydrophobic surfaces, where inertial-capillary motion is favored by liquids that do not strongly wet the solid [24]. Most importantly, the CL displacements associated with these large length scales are sufficient to overcome the micrometer-sized defects associated with surface roughness that can induce CL pinning and stick-slip behaviors. Figure 2 shows the time evolution of a mobile drop oscillating in the $[2, 0]$ mode, where comparing time 0 s to 0.31 s illustrates large CL displacements. Of course it is not possible to have a perfect $\Lambda = 0$ surface; however, for sufficiently small Λ, drop resonance $\hat{\Omega}$ is nearly identical to the fully mobile $\Lambda = 0$ case, as evidenced by the horizontal regions shown in Figure 1**d** for $0 \leq \Lambda \lesssim 1$, which plots $\hat{\Omega}$ against Λ for a typical experiment. We have measured Λ using the technique of Xia and Steen [25] for all substrates used in our experiments, finding that Λ falls within the shadowed region of Figure 1**d**. Given that our experiments fall within the lower frequency plateau region for all modes, we are comfortable in comparing our experimental results with the $\Lambda = 0$ theoretical predictions.

Experiment

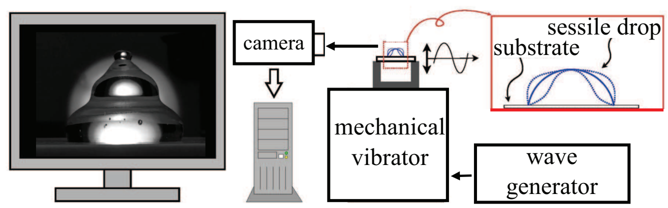

FIG. 3: Experimental schematic.

Experiments were conducted aboard the ISS Observation and Analysis of Smectic Islands in Space (OASIS) system within the OASIS bubble chamber, as schematically shown in Figure 3. A 10 mL water drop with density $\rho = 1$ g/mL, surface tension $\sigma = 72$ mN/m, and viscosity $\mu = 10^{-3}$Pa s is deposited onto a partially-wetting substrate via a syringe. Nine substrates were prepared with a wide range of wetting properties $\alpha, \alpha_a, \alpha_r, a$, given in Table I, where α and a were geometrically measured by fitting a circle to the drop shape at rest. These substrates were designed to be low-friction and produce freely moving contact-lines, with the exception of Substrate P_1 which was fabricated with a circular indentation of radius 1.5 cm to mechanically ‘pin’ the contact-line. The substrate is oscillated in the normal direction by a PASCO Scientific SF-9324 mechanical wave-driver with prescribed amplitude range $F_0 = 0.6$ - 1.7 mm and frequency f_d controlled via a PASCO WA-9867 sine wave generator, generating accelerations from 0.0002 g - 0.24 g. Motions are captured at 148 fps via a PixeLink M4-CYL high-speed camera backlit via LED lighting.

A frequency scan was performed for each substrate for a range of driving frequencies $f_d = 1 - 10$ Hz with a frequency interval of 0.2 Hz. Here we waited 5 seconds before proceeding to the next successive frequency. Near

TABLE I: Substrate identification table with wetting properties $\alpha, \alpha_a, \alpha_r$. Substrates labeled F_x denote free drop conditions, whereas Substrate P_1 is fabricated with a 1.5cm radius pinning site to produce pinned drop conditions.

ID	Substrate	Modification	$\alpha(^\circ)$	$\alpha_a(^\circ)$	$\alpha_r(^\circ)$	a(cm)
F_1	Silicon	PDMS	106	108	99	1.65
F_2	Silicon	Fluorosilane	114	121	90	1.59
F_3	Glass	PDMS	102	106	96	1.66
F_4	Glass	Fluorosilane	112	122	84	1.60
F_5	Teflon	Unsanded	115	116	77	1.57
F_6	Teflon	320 grit sanded	130	155	100	1.42
F_7	Teflon	240 grit sanded	143	163	62	1.23
F_8	Teflon	120 grit sanded	128	148	59	1.44
P_1	Silicon	Fluorosilane	135	N/A	N/A	1.35

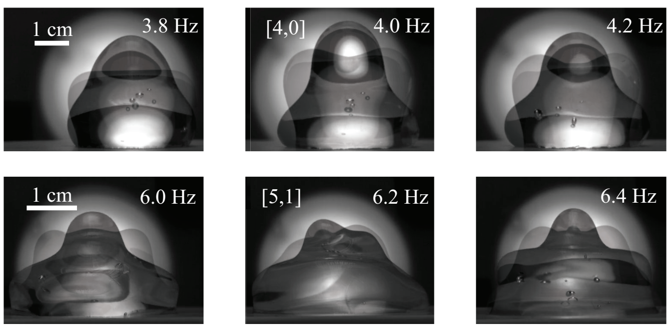

FIG. 4: Resonance identification from overlaid images for sequential driving frequencies. Top row: the $[4, 0]$ mode persists over the entire frequency range exhibiting maximal extension at resonance $f_d = 4.0$ Hz for Substrate F_4, whereas bottom row: the $[5, 1]$ mode exists only in a small frequency window at $f_d = 6.2$ Hz that lies between axisymmetric shapes for Substrate F_5.

resonance, the drop oscillates with fundamental mode shape $[k, l]$ described by theory [13]. Modal identification is achieved by comparing side-view perspective droplet shapes to theoretical predictions using two techniques. The first has been utilized in terrestrial-based drop vibration experiments [18, 23], where the magnitude of the interfacial disturbance from equilibrium is measured and resonance is defined by the largest such deflection. This technique is illustrated in the top row of Figure 4, where a series of drop images are overlaid at the prescribed driving frequency. Here it is clear the maximal deflection for the [4,0] mode occurs at 4.0 Hz. This techniques works well whenever the resonance frequency for that particular mode is isolated. However, in some cases, two or more modes $[k, l]$ may have nearly identical resonance frequencies. This is shown in the bottom row of Figure 4. Here the asymmetric [5,1] mode only appears at 6.2 Hz and lies in between an axisymmetric mode at slightly lower (6.0 Hz) and higher (6.4 Hz) frequencies. For this second technique, once a resonant mode shape is identified via comparison to predicted shape, the oscillation frequency f is determined via a Fast Fourier Transform with respect to time. Here in-house developed tracking algorithms were utilized to reduce image noise and to adequately resolve both the liquid/gas interface and contact-line region. We note that all observed motions are harmonic, i.e. the oscillation frequency is equal to the driving frequency $f = f_d$, which is distinguished from terrestrial-based experimental studies of pinned contact-line sessile drop vibrations, some of which exhibit a subharmonic response, $f = f_d/2$.

Results

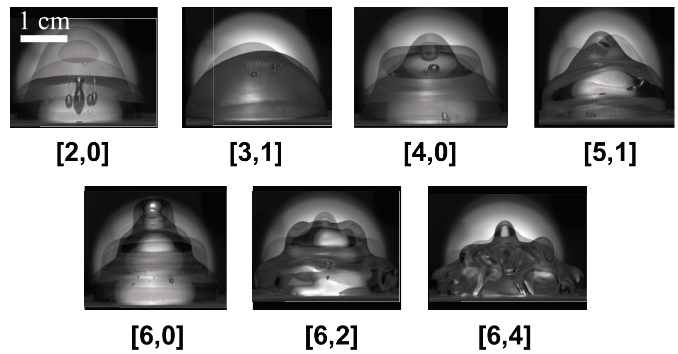

FIG. 5: Experimentally-observed modes $[k, l]$ overlaid throughout an oscillation cycle.

Figure 5 presents a catalogue of the experimentally-observed modes $[k, l]$, as described by the classification scheme of Steen et al. [15]. We note the zonal modes $[2, 0], [4, 0], [6, 0]$ were observed on every substrate tested, whereas the tesseral modes $[3, 1], [5, 1], [6, 2], [6, 4]$ were not. Several modes were undetected altogether, including sectoral modes $[2, 2], [3, 3], \cdots, [k, k]$, which we attribute to the discrete 0.2 Hz interval of the frequency scan. More specifically, if the resonance frequency for that particular mode lies within the frequency interval and has a small bandwidth then it is possible that this mode was skipped during the frequency scan. In addition, whenever two modes have nearly the same resonance frequency modal competition can occur, as described by Chang et al. [18], and in this case the lower energy mode saturates the droplet response making the higher energy mode nearly undiscoverable except in a small frequency range. Lastly, we note that poor lighting and droplet positioning could have played a role in modal discovery, as well as the practicalities of performing experiments aboard the ISS in a microgravity environment with corresponding time constraints. Despite these challenges, our experiments yielded a large data set over a range of hydrophobic-to-superhydrophobic wetting conditions $102^\circ < \alpha < 143^\circ$ with freely moving contact-lines.

Figure 6 plots the resonance frequency against the

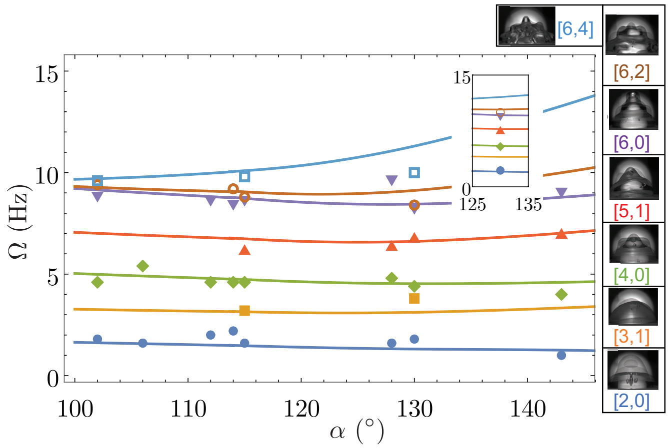

FIG. 6: Frequency (Hz) against static contact-angle $\alpha(^\circ)$ contrasting experiment (symbols) with theoretical predictions with free contact-lines $\Lambda = 0$ (solid lines) for modes $[k, l]$ on Substrates F_1-F_8. Inset is a plot of frequency Ω for Substrate P_1 for pinned drops. Experimental error ± 0.2 Hz is defined by the symbol size.

TABLE II: Resonant frequencies [Hz] contrasting free F_6 $\alpha = 130^\circ$ and pinned P_1 $\alpha = 135^\circ$ CLs.

Mode	[2,0]	[3,1]	[4,0]	[5,1]	[6,0]	[6,2]	[6,4]
F_6 (Hz)	1.8	3.8	4.4	6.8	8.2	8.4	10
P_1 (Hz)	2.2	-	5.4	7.6	9.4	10	-

contact-angle α contrasting experimental observations (symbols) with theoretical predictions (solid lines) from Bostwick and Steen [13] for free contact-lines $\Lambda = 0$. The figure inset corresponds to Substrate P_1 with pinned contact-line $\Lambda = \infty$. We note the excellent agreement between experiment and theory, especially for the zonal modes $[k, 0]$ over a large range of α. The higher energy modes $[6, 2]$, $[6, 4]$ tend to undershoot theoretical predictions as α deviates further from hemispherical $\alpha = 90^\circ$, which is consistent with other studies [18]. The experimental frequencies agree with theory within 9%, and excluding the $[2, 0]$ mode, agree within 4.3% at maximum with most observations falling within 1%. Given the potential sources of error described above, this excellent agreement suggests 1) the experiments indeed produce drops with freely moving CLs (corroborating independent image analysis) and 2) the model captures the essential physics of oscillating sessile drops with freely-moving CLs.

It is interesting to contrast the results for Substrates F_6 and P_1, given they have similar static contact angle $\alpha = 130^\circ - 135^\circ$ but dramatically different contact-line dynamics. Substrate F_6 produces fully mobile $\Lambda = 0$ contact-lines, whereas Substrate P_1 produces fully immobile $\Lambda = \infty$ contact-lines, thus encompassing both extremes of the more general contact-line dynamics $\Lambda \neq 0, \infty$. Table II shows the resonance frequencies for the pinned drop (Substrate P_1) are always larger than that for the free drop (Substrate F_6) consistent with our mathematical understanding that a pinned contact-line boundary condition tends to 'constrain' the drop more than the free contact-line boundary condition from an energy variational sense [26]. Our experimental results verify this understanding of the contact-line physics.

Lastly, we note all of our experiments produced drop resonances with a harmonic response, in contrast to terrestrial-based experimental studies of pinned drops [17, 18], which exhibited more complicated dynamics; the zonal modes $[k, 0]$ responded harmonically but the sectoral $[k, k]$ and tesseral $[k, l \neq k]$ modes responded subharmonically. Typically, a subharmonic droplet response is associated with the onset of Faraday waves with corresponding onset acceleration, i.e. the drop interface remains undeformed until a critical (and finite) forcing acceleration is reached upon which the wave is formed on the interface [27]. This is commonly referred to as Faraday wave onset. In contrast, a harmonic droplet response typically occurs for all values of the driving acceleration as axisymmetric traveling waves are excited from the contact-line and constructively or destructively interfere with one another at the drop apex creating a standing wave pattern in the form of a zonal mode. Given our observations that all modes respond harmonically, it is reasonable to conclude the forcing amplitudes used in our experiments are smaller than required for Faraday wave onset. This is most likely related to the i) low drop weights inherent in microgravity and ii) the comparably small capillary pressures, which scale inversely with the drop radius r^{-1}, that must be overcome to excite shape oscillations.

Discussion

We have reported the results of an experimental study of oscillating sessile drops on hydrophobic surfaces over a wide range of wetting properties. The experiments were conducted in the microgravity environment aboard the ISS enabling fully mobile contact-line dynamics with corresponding physics, which have heretofore been unrealized in terrestrial-based experiments. The large capillary lengths possible in microgravity permitted the use of centimeter-scale drops with CL deformation able to overcome the typical micrometer-size surface defects which are known to cause contact-line pinning in millimeter-size water drops. Resonance frequencies were measured for seven mode shapes and compared with theoretical predictions, showing good agreement, thus suggesting our model adequately captures the physics of mobile contact-lines for oscillating drops.

Fully-mobile contact-line dynamics are a limiting case of the more general, and often increasingly complex, area of dynamic wetting, which can yield motions such as stick-slip [28], air entrainment, among others [29]. The Davis-Hocking model (1) is often invoked in theoretical studies involving contact-line motions so much that the question has been recently asked 'is the contact-line mobility Λ a material parameter?' that can be measured [24, 30]. This is an open question, particularly for capillary-ballistic motions characterized by high Reynolds number Re and moderate Weber number We, $\mathrm{Re} > \sqrt{\mathrm{We}}$, defining the inertial spreading regime. Our study helps to answer this question by producing experimental results for the most sought-after extreme $\Lambda = 0$ (fully-mobile CL) which when combined with prior results for the other extreme $\Lambda = \infty$ (pin CL) will aid in designing future studies to explore the finite Λ regime.

Recent advances in manufacturing has led to the fabrication of 'designer surfaces' with controllable wetting properties through combinations of surface chemistry, roughness, and microstructure [31, 32]. The ever shrinking length scale of surface defects in these fabrication processes will inevitably lead to the realization of drop motions with fully mobile CLs under terrestrial conditions [33, 34]. Numerous microgravity technologies involve free CL motions including wickless heat pipes for thermal management [35], fuel management devices [36], and more general handling of fluids via capillary drainage [37, 38], some of which are mission critical. For example, in the NEAR anomaly spreading of hydrophobic fuels, e.g. a 'green' hydroxyl ammonium nitrate fuel/oxidizer blend AF-M315E [39], during dynamic flight maneuvers sent the spacecraft into safety mode, thereby losing communication for approximately 27 hours and delaying the intended mission by over a year [40]. Given the criticality of these current and future areas of technology, our canonical study of sessile drop motions with free CLs is both essential and timely to the field of inertial wetting dynamics.

Acknowledgements Special thanks to NASA astronauts Kathleen Rubins and Michael Hopkins for their patience and insight in performing the experiments. Thanks to Jonathan Ludwicki for experimental design assistance. The authors acknowledge the role of Professor P.H. Steen in leading this research, and note his passing before the time of publication. We are honored to be able to continue this work and bring it to the field.

We gratefully acknowledge support from NSF grants 1530522, 1637960 and 1935590 and NASA Grant 80NSSC19K0406.

[1] E. A. Costner, M. W. Lin, W. L. Jen, and C. G. Willson, Annual Review of Materials Research **39**, 155 (2009).
[2] B. Derby, Engineering **1**, 113 (2015).
[3] J. Li, Y. Hou, Y. Liu, C. Hao, M. Li, M. K. Chaudhury, S. Yao, and Z. Wang, Nature Physics **12**, 606 (2016).
[4] S. T. Thoroddsen, M.-J. Thoraval, K. Takehara, and T. Etoh, Physical review letters **106**, 034501 (2011).
[5] G. Riboux and J. M. Gordillo, Physical review letters **113**, 024507 (2014).
[6] K. Cardin, S. Wang, O. Desjardins, and M. Weislogel, Physical Review Fluids **6**, 014003 (2021).
[7] N. J. Cira, A. Benusiglio, and M. Prakash, Nature **519**, 446 (2015).
[8] T.-S. Wong, S. H. Kang, S. K. Tang, E. J. Smythe, B. D. Hatton, A. Grinthal, and J. Aizenberg, Nature **477**, 443 (2011).
[9] P. Juuti, J. Haapanen, C. Stenroos, H. Niemelä-Anttonen, J. Harra, H. Koivuluoto, H. Teisala, J. Lahti, M. Tuominen, J. Kuusipalo, et al., Applied Physics Letters **110**, 161603 (2017).
[10] C. Zhang, S. Adera, J. Aizenberg, and Z. Chen, ACS Applied Materials & Interfaces **13**, 15901 (2021).
[11] L. M. Hocking, Journal of Fluid Mechanics **179**, 253 (1987).
[12] S. H. Davis, Journal of Fluid Mechanics **98**, 225 (1980).
[13] J. B. Bostwick and P. H. Steen, Journal of Fluid Mechanics **760**, 5 (2014).
[14] T. MacRobert, *Spherical Harmonics* (Pergamon, New York, NY, 1967).
[15] P. H. Steen, C. T. Chang, and J. B. Bostwick, Proceedings of the National Academy of Sciences of the United States of America **116**, 4849 (2019).
[16] L. Rayleigh, Proc. R. Soc. Lond. **29**, 71 (1879).
[17] C.-T. Chang, J. B. Bostwick, P. H. Steen, and S. Daniel, Phys. Rev. E **88**, 023015 (2013).
[18] C.-T. Chang, J. Bostwick, S. Daniel, and P. Steen, Journal of Fluid Mechanics **768**, 442 (2015).
[19] D. t Mannetje, S. Ghosh, R. Lagraauw, S. Otten, A. Pit, C. Berendsen, J. Zeegers, D. van den Ende, and F. Mugele, Nature communications **5**, 1 (2014).
[20] G. Fang, W. Li, X. Wang, and G. Qiao, Langmuir **24**, 11651 (2008).
[21] O. A. Basaran and D. W. DePaoli, Physics of Fluids **6**, 2923 (1994).
[22] J. S. Sharp, Soft Matter **8**, 399 (2012).
[23] V. R. Kern, J. B. Bostwick, and P. H. Steen, Journal of Fluid Mechanics **923**, 1 (2021).
[24] Y. Xia and P. H. Steen, Journal of Fluid Mechanics **841**, 767783 (2018).
[25] Y. Xia and P. H. Steen, npj Microgravity **6**, 1 (2020).
[26] J. B. Bostwick and P. H. Steen, Annual Review of Fluid Mechanics **47**, 539 (2015).
[27] M. Faraday, Philosophical transactions of the Royal Society of London pp. 299–340 (1831).
[28] P. Brunet, J. Eggers, and R. D. Deegan, Phys. Rev. Lett. **99**, 144501 (2007).
[29] J. H. Snoeijer and B. Andreotti, Annual Review of Fluid Mechanics **45**, 269 (2013).
[30] J. M. Ludwicki and P. H. Steen, npj Microgravity p. accepted (2022).
[31] C. Jothi Prakash and R. Prasanth, Journal of Materials Science **56**, 108 (2021).
[32] H. Li, A. Li, Z. Zhao, M. Li, and Y. Song, Small Structures **1**, 2000028 (2020).
[33] Q. Li, D. Wu, and Z. Guo, Soft matter **15**, 6803 (2019).
[34] J. Chi, X. Zhang, Y. Wang, C. Shao, L. Shang, and Y. Zhao, Materials Horizons **8**, 124 (2021).
[35] A. Kundan, J. L. Plawsky, P. C. Wayner Jr, D. F. Chao, R. J. Sicker, B. J. Motil, T. Lorik, L. Chestney,

J. Eustace, and J. Zoldak, Physical Review Letters **114**, 146105 (2015).

[36] D. Levine, B. Wise, R. Schulman, H. Gutierrez, D. Kirk, N. Turlesque, W. Tam, M. Bhatia, and D. Jaekle, Journal of Propulsion and Power **31**, 429 (2015).

[37] J. McCraney, M. Weislogel, and P. Steen, Fluids **5**, 207 (2020).

[38] J. McCraney, M. Weislogel, and P. Steen, npj Microgravity **7**, 1 (2021).

[39] M. Martin, J. Smolen, M. Weislogel, J. Thomas, and E. Peterson, in *JANNAF* (2019).

[40] E. J. Hoffman, W. Ebert, M. Femiano, H. Freeman, C. Gay, C. Jones, P. Luers, and J. Palmer, Applied Physics Laboratory, Johns Hopkins University, Tech. Rep (1999).